Investigation of near-field propagation properties of mosaic grating based compressor for kilojoule petawatt laser system

Pengfei Huang[1,2], Zuocai Jiang[1], Youen Jiang[1], Xuechun Li[1], Jianqiang Zhu[1], Yanli Zhang[1*], Pengqian Yang[1*] and Liangyu Wang[1]

[1]*National Laboratory on High Power Lasers and Physics, Shanghai Institute of Optics and Fine Mechanics, Chinese Academy of Sciences, Shanghai 201800, China*

[2]*University of Chinese Academy of Sciences, Beijing 100049, China*

Abstract Large-aperture gratings are core components for pulse compression in kilojoule petawatt laser systems. The wavefront or amplitude error originated from fabrication and assembly of these gratings can be transformed into near-field modulation during propagation of the laser pulse. In severe cases, near-field modulation would induce laser damage on gratings and downstream optics. In this study, a three-dimensional near-field propagation model is developed based on ray tracing and diffraction propagation theory, allowing to quantify the effect of each grating in the compressor independently. We investigate near-field propagation properties of mosaic grating based compressor in detail, the impacts of periodic wavefront error and mosaic gap error of mosaic grating on near-field modulation is analyzed and evaluated, with two measured wavefronts introduced for further analysis. This work offers theoretical insights for estimating the fabrication requirement of gratings and reducing the risk of laser damage.

Key words: Petawatt laser, Mosaic grating, Mosaic gap error, Near field

---

Correspondence to: Qinghe Rd. No.390. Shanghai. Email: zhangyl@siom.ac.cn, yangpengqian@siom.ac.cn.

This peer-reviewed article has been accepted for publication but not yet copyedited or typeset, and so may be subject to change during the production process. The article is considered published and may be cited using its DOI.
This is an Open Access article, distributed under the terms of the Creative Commons Attribution licence (https://creativecommons.org/licenses/by/4.0/), which permits unrestricted re-use, distribution, and reproduction in any medium, provided the original work is properly cited.
10.1017/hpl.2025.10050

https://doi.org/10.1017/hpl.2025.10050 Published online by Cambridge University Press

I. INTRODUCTION

The kilojoule petawatt (PW) laser system produces kJ pulses with durations ranging from hundreds of femtoseconds to picoseconds. It plays a critical role in high-energy-density physics research, including laser accelerators[1], inertial confinement fusion (ICF)[2, 3], and laboratory astrophysics[4]. In order to generate kilojoule PW laser, Chirped Pulse Amplification (CPA) technology[5] is indispensable, it prevents high peak powers within the amplifier by temporally stretching the pulse before amplification, then recompressing the amplified pulse with a grating compressor to produce a short, high peak power pulse. In typical kilojoule PW laser systems, successive amplification expands the beam aperture to hundreds of millimeters, requiring gratings size along the dispersion direction exceeding one meter in compressors.

Many strategies were proposed to meet the requirement of pulse compression[6-9], there are mainly two approaches have been implemented to address the constraint of grating size in current kilojoule PW laser systems around the world. The first is the synthetic aperture compression scheme, which crops the beam into several beamlets for independent compression. The NIF ARC system adopts this approach[10], four groups of $0.91\mathrm{m}\times0.45\mathrm{m}$ gratings are arranged in a 2×2 configuration to form four independent compressors to compress four beamlets. The LMJ-PETAL system divides the compression system into two stages[11], and employs this approach in the second stage. While synthetic aperture compression scheme reduces the demand of grating size, it comes with energy loss. Another approach involves mechanical or optical grating mosaic to manufacture meter-scale gratings directly to mitigate the problem, for example, OMEGA EP system mechanically tiles three $0.47\mathrm{m}\times0.43\mathrm{m}$ gratings[12], LFEX system mechanically tiles two $0.91\mathrm{m}\times0.42\mathrm{m}$ gratings[13]. In mechanical tiling solution, each element grating is fabricated on a separate substrate. Alternatively, the SG-II UP PW picosecond system

https://doi.org/10.1017/hpl.2025.10050 Published online by Cambridge University Press

uses $1.4\text{m}\times0.42\text{m}$ optical mosaic gratings made by consecutive exposures of a single substrate[14, 15], this method avoids the requirement of multiple high-accuracy control and adjustments of mechanical tiling method[12], but the mosaic gap error degrades the beam quality[7, 16].

During pulse propagation within the compressor, wavefront or amplitude error originated from fabrication and assembly of gratings can significantly degrade beam quality. Li et al.[17] discovered that periodic wavefront error introduced by grating fabrication lead to complex spatio-temporal coupling effect for femtosecond laser. Š. Vyhlídka.[18] analyzed the impacts of gap induced amplitude errors on near field at G4 in the femtosecond PW laser system. For kilojoule PW laser with relatively longer duration, researchers primarily focus on the degradation of spatial beam quality caused by these errors. The far-field degradation has received a lot of attention since it directly affects the output capability. Qiao et al.[19] analyzed focal-spot degradation from all combined tiling errors of the OMEGA-EP system compressor. Zhang et al.[20] evaluated tolerances of input wavefront error and grating deformation by far-field quality. Recently, the near-field modulation induce by grating errors started to gain more attention, it can induce laser damage on the last grating and downstream optics as these components are subject to the highest fluence, which is a main factor limiting the output capability[21, 22]. Koch et al.[23] pointed out that periodic mid-spatial frequency wavefront errors will cause dramatic near-field modulations, but their analysis was limited to single gratings, similarly, Zhang et al.[24] only examined the near-field degradation caused by diffraction effects of tiling gap for single tiled gratings. In 2007, H. Huang et al.[25] pointed out that the spatial dispersion can smooth the fluence modulation at G4 induced by G2 and G3 tiled gaps in OMEGA-EP laser system, but they did not specify the exact smoothing properties. To our best knowledge, the comprehensive near-field propagation properties of mosaic grating based compressor has not been completely revealed yet.

https://doi.org/10.1017/hpl.2025.10050 Published online by Cambridge University Press

In this paper, we develop a three-dimensional near-field propagation model for the compressor of the SG-II UP PW picosecond system, utilizing ray tracing and diffraction propagation theories. From the perspective of the entire compressor, the effects of periodic wavefront errors, mosaic gap errors of the first three exposure mosaic gratings (G1-G2-G3) on the near field at the last grating (G4) are evaluated, with two measured wavefronts introduced to further analyze for G1. With the goal of reducing near-field modulation to mitigate the risk of laser induced damage of G4, our study determines tolerances of both periodic wavefront errors and mosaic gap error.

II. THEORETICAL MODEL

2.1 Overview of model

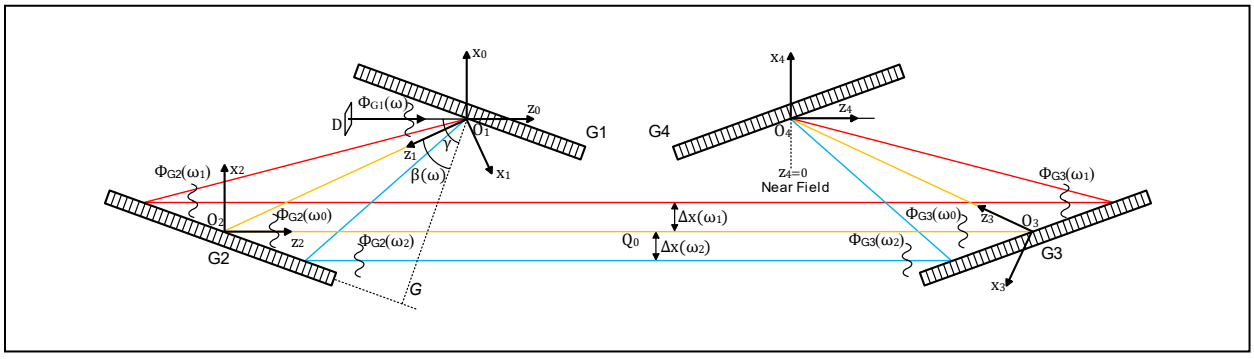

Figure 1. Schematic of broadband pulse propagation model for grating compressor.

A 3D model of pulse near-field propagation within the compressor was established by Fresnel scalar diffraction theory combined with geometric optics and coordinate transformation, the configuration of the compressor and the coordinates are shown in Figure 1, it is a typical one-pass Treacy configuration[26], but consists of four identical mosaic gratings. For kilojoule PW laser, neglecting the spatio-temporal couplings (STCs)[27], the incident field is written as:

https://doi.org/10.1017/hpl.2025.10050 Published online by Cambridge University Press

$$\begin{cases} U_0(x_0, y_0, z_0 = 0, \omega) = b_0 A(x_0, y_0) A(\omega) \exp[-i\varphi(\omega)] \\ A(x_0, y_0) = \exp\{-2^{N-1}[(\frac{|x_0|}{D})^N + (\frac{|y_0|}{D})^N]\} \\ A(\omega) = \exp[-2(\frac{\omega}{\Delta\omega})^2] \end{cases} \tag{2.1}$$

Where D is full width at e^{-2} maximum intensity of the super-Gaussian spatial profile, a plane wave is assumed. $\Delta\omega$ is full width at e^{-2} maximum intensity of the Gaussian spectral profile, $\varphi(\omega)$ is spectral phase, b_0 is energy factor. The incident pulse is diffracted by G1 and divided into multiple sub-beams as different spectral components ω of beam transmission in different paths, γ is the incident angle, $\beta(\omega)$ is the diffraction angle of ω, the grating law is[28]:

$$\sin\gamma + \sin\beta(\omega) = \frac{2\pi c}{\omega d} \tag{2.2}$$

Where d is grating period. Considering first-order approximation[29], the diffracted field can be expressed as:

$$U_1(x_1, y_1, 0, \omega) = A_{G1} b_1 U_0(\alpha x_1, y_1, \omega) \exp(i\Phi_{G1}) \tag{2.3}$$

Here the grating is treated as a specialized mirror, its reflection direction is dependent on ω of broadband pulse. A_{G1}, Φ_{G1} are amplitude error and wavefront error introduced by fabrication errors of G1, respectively. Where b_1 is normalized energy factor, $\alpha = -\cos\gamma / \cos\beta(\omega)$ is coordinate transformation factor along the dispersion direction, i.e., the x direction. It is noted that the diffraction angle of G1 is equal to the incident angle of G2, similarly for two downstream gratings, the grating law is utilized to trace the center rays of all sub-beams within the compressor, these center rays are used as z-axis and baselines for the diffraction propagation of corresponding

https://doi.org/10.1017/hpl.2025.10050 Published online by Cambridge University Press

sub-beams. According to the scalar diffraction theory[30], the field of ω on the surface of G2 can be expressed as:

$$U_{1P}(x_1', y_1', P(\omega), \omega) = \frac{\exp(-jkP(\omega))}{-j\lambda P(\omega)} \exp[\frac{-jk}{2P(\omega)}(x_1'^2 + y_1'^2)] \iint_{\infty} U_1(x_1, y_1, 0, \omega) \times \exp[\frac{-jk}{2P(\omega)}(x_1^2 + y_1^2)] \exp[\frac{jk}{P(\omega)}(x_1' x_1 + y_1' y_1)] dx_1 dy_1 \quad (2.4)$$

Where $k = \omega / c$ is wave number, G is perpendicular distance between G1 and G2, $P(\omega) = G \sec\beta(\omega)$ is slant distance for ω, as illustrated in Figure 1. After that, the field is diffracted by G2 and modulated by A_{G2}, Φ_{G2}, then propagating to G3 and being modulated by A_{G3}, Φ_{G3}. Notably, the intersection positions of G2, G3 surface with center ray of individual sub-beam possess *x*-axis shifts due to angular dispersion. Since the sub-beams only illuminate a portion of the grating, the wavefront of each sub-beam is a segment of overall diffracted wavefront, the *x*-axis shifts can be described as the interval between center rays of ω and ω_0 within G2-G3[17]:

$$\Delta x(\omega) = G[\tan\beta(\omega) - \tan\beta(\omega_0)]\cos\gamma \quad (2.5)$$

With this parameter, the optical pathlength within G2-G3 for ω can be expressed as:

$$Q(\omega) = Q_0 + 2\Delta x(\omega)\tan\gamma \quad (2.6)$$

Where Q_0 is the distance between G2 and G3 for ω_0. Finally, the field is transmitted from G3 to G4, which is the reverse process of that for G1-G2 grating pair. The near-field distribution $U_{4NF}(x_4, y_4, 0, \omega)$ at G4 is obtained, the laser fluence can be expressed as:

https://doi.org/10.1017/hpl.2025.10050 Published online by Cambridge University Press

$$F_{NF}(x_4, y_4) = \int |U_{4NF}(x_4, y_4, 0, \omega)|^2 \, d\omega \tag{2.7}$$

The spatio-temporal distribution at G4 can be obtained by the inverse Fourier transform of $U_{4NF}(x_4, y_4, 0, \omega)$:

$$U_{4NF}(x_4, y_4, 0, t) = \frac{1}{2\pi} \int_{-\infty}^{+\infty} U_{4NF}(x_4, y_4, 0, \omega) \exp(i\omega t) d\omega \tag{2.8}$$

In general, the propagation model described above can calculate the spatio-spectral distribution at any position within the compressor by establishing a unified coordinate and undergoing coordinate rotation. While this study primarily focuses on near-field modulation at G4 induced by errors of upstream grating to investigate control requirements of these errors as G4 suffers the greatest risk of laser-induced damage.

2.2 Periodic wavefront error

For holographic grating, the diffracted wavefront errors are originated from groove errors caused by imperfect exposure system and surface imperfection[31], and the periodic wavfront errors are introduced during the fabrication process[7], for example, small-tool polishing of the substrate and the exposure system imperfection. The 2D periodic wavefront error can be expressed as[32]:

$$\Phi(x, y, \omega) = \mathrm{k} \frac{H}{2} \left[\frac{\sin(2\pi \frac{x}{T}) + \sin(2\pi \frac{y}{T})}{2} \right] \tag{2.9}$$

Where H is peak-to-valley (PV) value of wavefront error, T is spatial period, the periods in two directions are assumed to be equal, the variation of PV value with ω is neglected for the narrowband laser pulse. Utilizing the parameter in Eq. (2.5), the wavefront error can be described

https://doi.org/10.1017/hpl.2025.10050 Published online by Cambridge University Press

as $\Phi_{G1}(x_1, y_1, \omega)$ with an arbitrary frequency ω for G1, but $\Phi_{G2}(x_2 - \Delta x(\omega), y_2, \omega)$ for G2 and $\Phi_{G3}(x_3 - \frac{\Delta x(\omega)}{\alpha}, y_3, \omega)$ for G3.

2.3 Mosaic gap error

As mentioned above, mosaic gap error is an inherent limitations of grating mosaic techniques, including amplitude error and phase jump. The amplitude error not only degrades the temporal contrast of pulse[33, 34]， but also causes near-field modulation by hard edge diffraction. SG-II UP PW picosecond system compressor utilizes $1.4\text{m} \times 0.42\text{m}$ grating with two mosaic gaps located at $1/3$，$2/3$ of its length, the amplitude error function for these gaps is given by:

$$A(x, y, \omega) = 1 - [rect(\frac{x + \frac{L}{6}\cos\beta(\omega)}{\text{w}\cos\beta(\omega)}) + rect(\frac{x - \frac{L}{6}\cos\beta(\omega)}{\text{w}\cos\beta(\omega)})] \tag{2.10}$$

Where w represents the gap width, L denotes the grating length, and $\text{w}\cos\beta(\omega)$ is corresponding gap width on the diffracted beam plane. Besides, the diffraction angle at G2 is γ, so the corresponding gap width is $\text{w}\cos\gamma$. Similar to wavefront error, the amplitude error function for G1 is $A_{G1}(x_1, y_1, \omega)$, while for G2 and G3 are $A_{G2}(x_2 - \Delta x(\omega), y_2, \omega)$ and $A_{G3}(x_3 - \frac{\Delta x(\omega)}{\alpha}, y_3, \omega)$, respectively. Moreover, the gap induced wavefront errors such as phase jump are dependent on the grating fabrication process, their impacts are assessed through two wavefronts measured by an interferometer.

https://doi.org/10.1017/hpl.2025.10050 Published online by Cambridge University Press

III. IMPACTS OF ERRORS ON NEAR FIELD AT G4

3.1 Simulation parameters

The near-field fluence modulation index defined as maximum value of fluence profile divided by its average value[35], is adopted to evaluate the impact of two types of errors on the near field at G4 (hereafter referred to as NF4). Based on the status of SG-II UP PW picosecond system, the simulated pulse possesses a center wavelength of 1053nm and a bandwidth (FWHM) of 3.8nm. The input beam of the compressor is 10-order super-Gaussian with a zero-intensity area (at 1% maximum intensity) of $320\times320\text{mm}^2$, the energy of output pulse duration is 1.2KJ@10ps. The spectral sampling window is set as 18nm centered in 1053nm, the spatial sampling window are $380\text{mm}\times380\text{mm}$. The sampling points are $4096,4096,512(x,y,\lambda)$ for fluence calculation, while $512,512,512(x,y,\lambda)$ for laser peak power calculation. The groove density of the grating is 1740g/mm, the incident angle is 71°, the perpendicular distance G of each grating pair is 2146mm, the optical pathlength between G2 and G3 for ω_0 is 10617mm. To facilitate analysis, the near-field modulation index of the input pulse is set to be 1, representing an ideal case, and the input energy is assumed to be 1.2KJ.

https://doi.org/10.1017/hpl.2025.10050 Published online by Cambridge University Press

3.2 NF4 fluence modulation induced by periodic wavefront errors

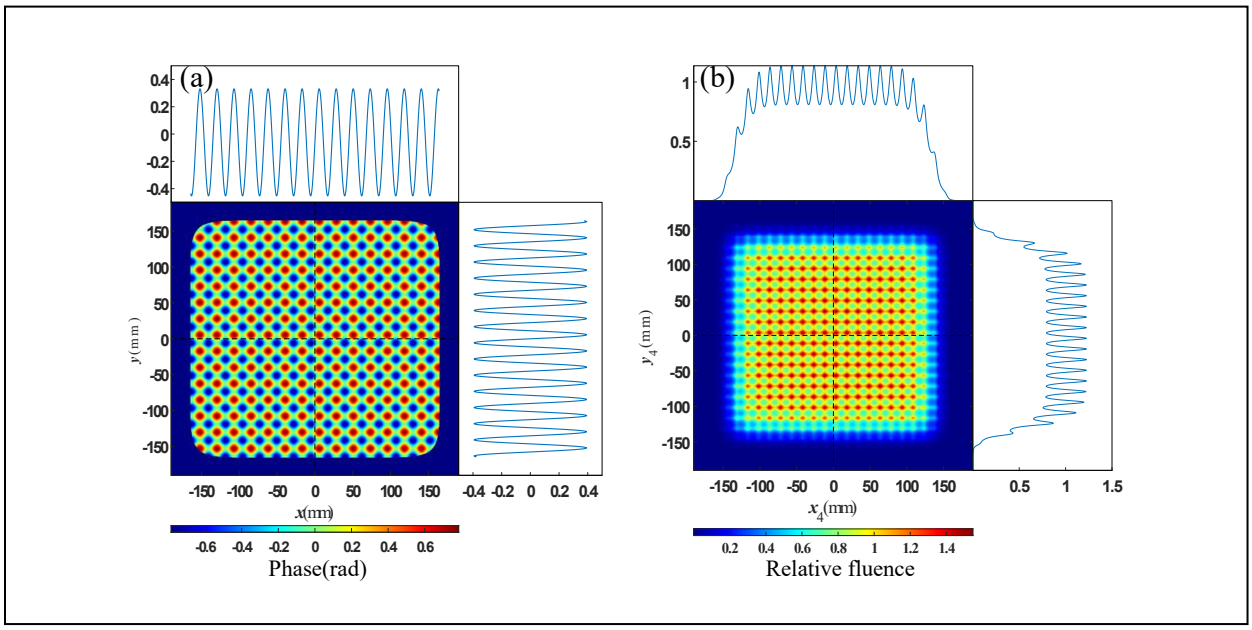

Figure 2. NF4 fluence modulation induced by the periodic wavefront error Φ_{G1} with T=15mm, H=λ/4. (a) Accumulation of Φ_{G1} over ω at the input beam plane. (b) NF4 fluence modulation induced by Φ_{G1}.

Figure 2 shows the 2D NF4 fluence modulation induced by the 2D periodic wavefront error of G1 with $T=15\text{mm}$, $H=\lambda/4$. It can be observed that periodic wavefront error results in periodic NF4 fluence modulation, the maximum modulation index has reached about 1.55, this phenomenon is known as the Talbot effect[23], it results in similar distributions of NF4 fluence and the accumulation of Φ_{G1} over ω. The periods of wavefront errors in the two directions are assumed to be identical, but the diffracted beam is broaden along the x direction due to $\beta(\omega)<\gamma<90^{\circ}$, which represents the periods of wavefront vary with ω after diffraction, but this variation is compensated at NF4. In a word, the diffracted wavefront can be equivalent to the input wavefront for G1, and the input wavefront is directly mapping to distribution of NF4 fluence.

The NF4 fluence modulations caused by Φ_{G2} or Φ_{G3} with $T=15\text{mm}$, $H=\lambda/4$ are

https://doi.org/10.1017/hpl.2025.10050 Published online by Cambridge University Press

displayed on Figure 3. As described in Section2, Φ_{G2} and Φ_{G3} possess ω-dependent shift along the dispersion direction, it indicates that the initial phase of periodic wavefront for individual sub-beam varies with ω. To evaluate the effects of wavefront errors on NF4 fluence, Φ_{G2} and Φ_{G3} of each sub-beam are accumulated over ω in the same aperture as the sub-beams are recombined at NF4. The summed result of the wavefronts are smoothed along the x direction due to the different initial phases. As a result, the fluence modulation are smoothed along the x direction, which can be seen in Figure 3 (b), (d). It is important to note that the accumulations of wavefront errors are fictitious distributions without physical significance, but they provide representations of the induced fluence modulation characteristics.

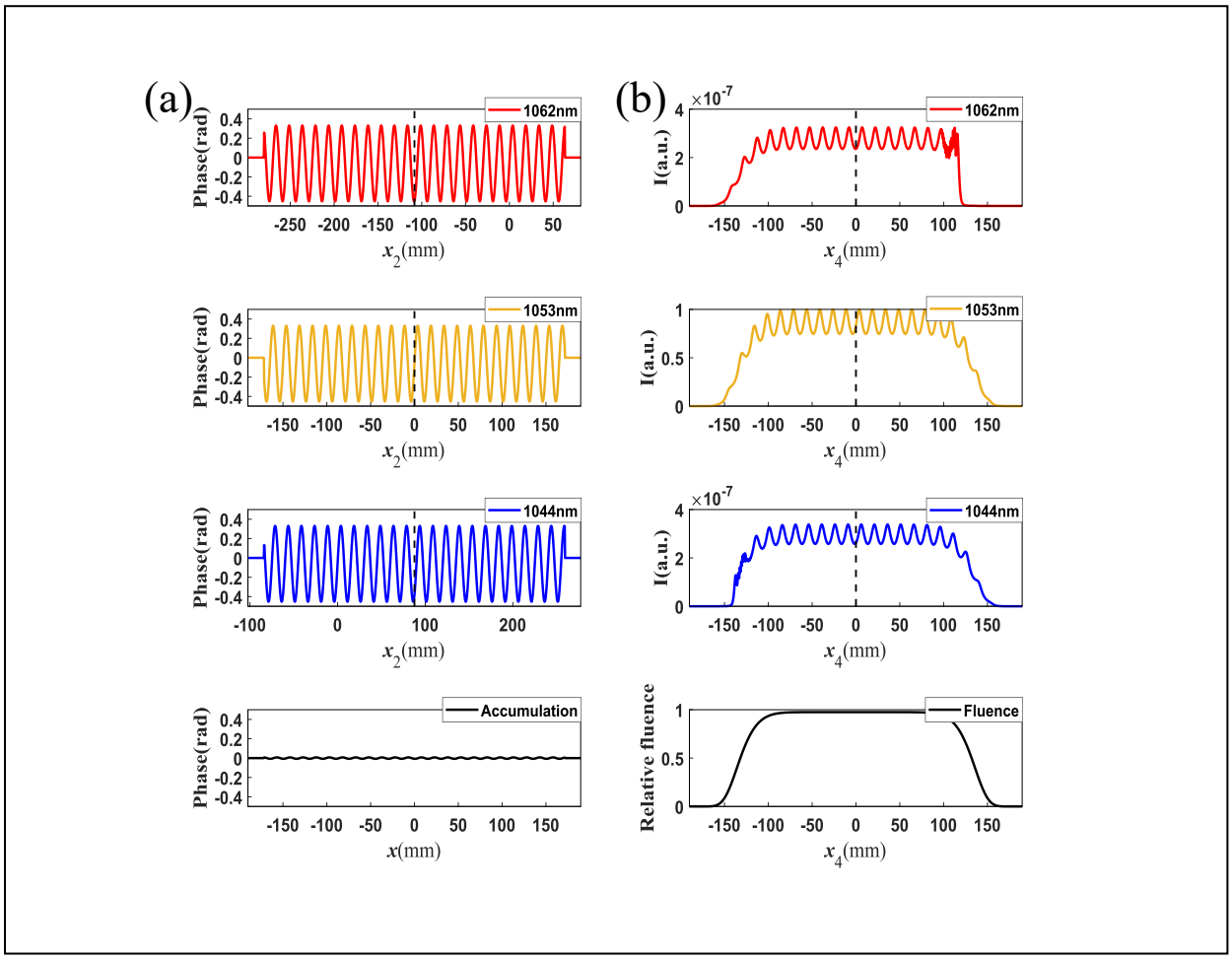

https://doi.org/10.1017/hpl.2025.10050 Published online by Cambridge University Press

Figure 3. NF4 fluence modulation induced by the periodic wavefront errors Φ_{G2} or Φ_{G3} with $T=15\text{mm}, H=\lambda/4$. (a) Accumulation of Φ_{G2} over ω in the same aperture. (b) NF4 fluence modulation induced by Φ_{G2}. (c) Accumulation of Φ_{G3} over ω in the same aperture. (d) NF4 fluence modulation induced by Φ_{G3}.

Figure 4 exhibits the NF4 intensity distributions induced by Φ_{G2} in different spectral components, the distortions of the intensity arise from spectral clipping of the compressor. It can be seen that the intensity modulation of each sub-beam is similar to the distribution of Φ_{G2}, which is the features of the Talbot effect, the different initial phases of Φ_{G2} result in different intensity distribution. Ultimately, the fluence modulation are smoothed along the dispersion direction. This interesting property can significantly mitigate fluence modulation induced by Φ_{G2} and Φ_{G3}, in the case of $T=15\text{mm}, H=\lambda/4$, the modulation index is only about 1.2 for Φ_{G2} and 1.05 for Φ_{G3}, much less than 1.7 for Φ_{G1}. Additionally, it can be observed that the NF4 peak fluence caused by Φ_{G2} are higher than that caused by Φ_{G3}, it is evident that an increased propagation distance can exacerbate the NF4 fluence modulation induced by wavefront errors under present working-distances.

https://doi.org/10.1017/hpl.2025.10050 Published online by Cambridge University Press

1

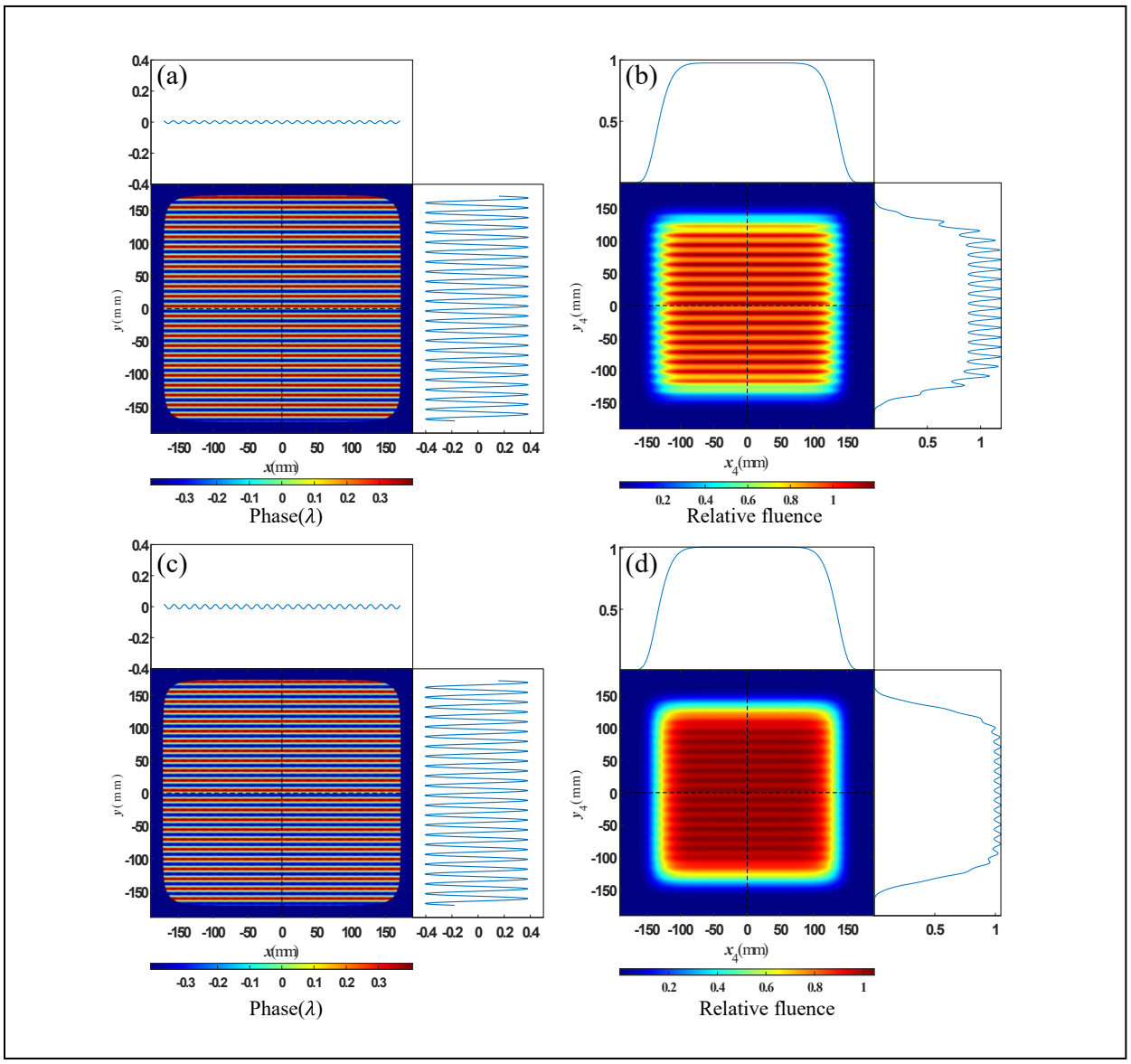

2 Figure 4. (a) The distributions of Φ_{G2} along the x_2 direction with $y_2 = 0$ for different

3 wavelengths, the black line represents the accumulated result of Φ_{G2}. (b) The resulting NF4

4 intensity distribution in different wavelengths along the x_4 direction with $y_4 = 0$, and the fluence

5 along x_4 direction is displayed at the bottom.

https://doi.org/10.1017/hpl.2025.10050 Published online by Cambridge University Press

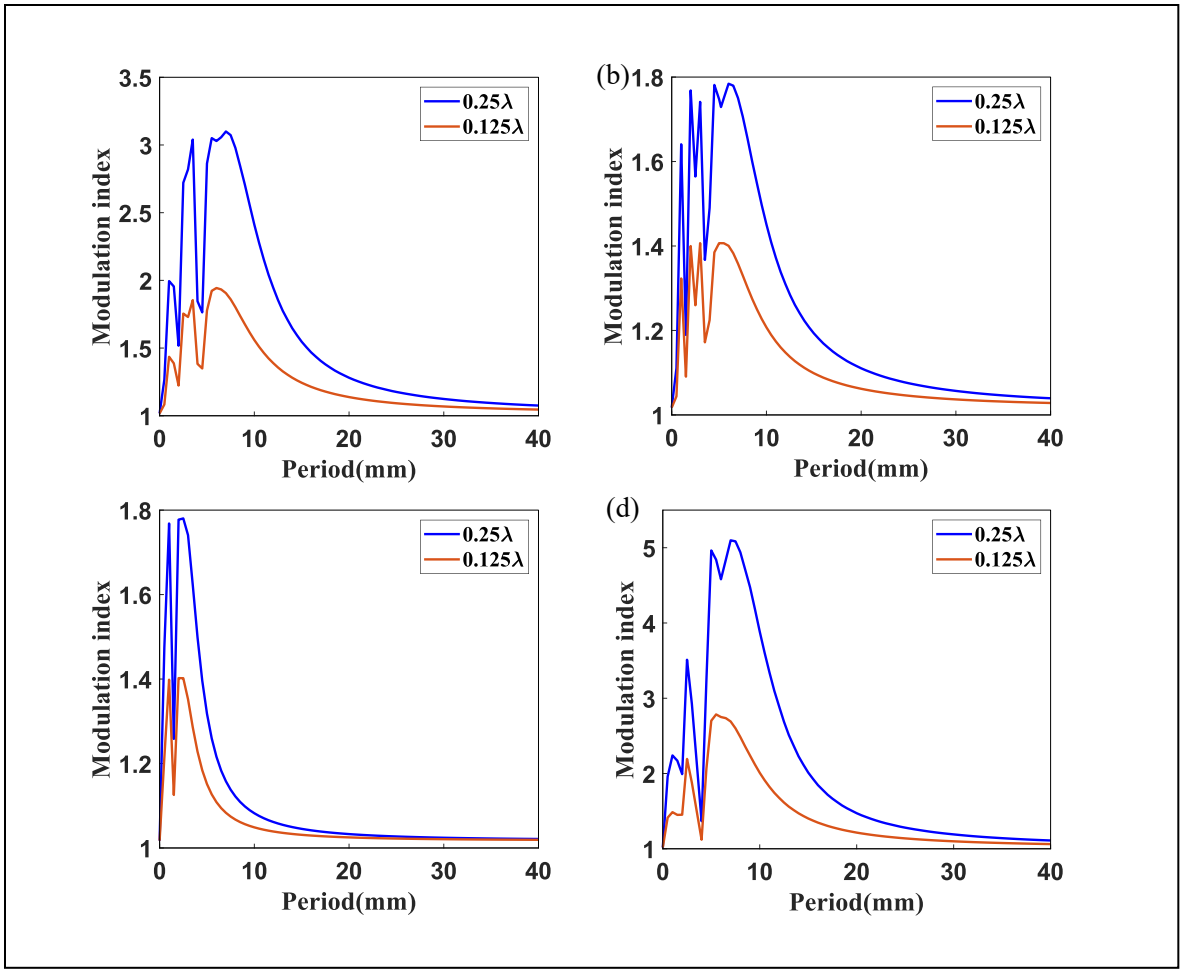

Figure 5. NF4 fluence modulation induced by (a) Φ_{G1}, (b) Φ_{G2}, (c) Φ_{G3}, (d) periodic wavefront errors of all upstream gratings, with $T = 0.5-40\text{mm}, H = \lambda/4$ or $\lambda/8$.

To study the effects of different PV values and periods of periodic wavefront errors for the first three gratings on NF4, considering a period range of $0.5-40\text{mm}$ with an interval of 0.5mm, $T = 0$ corresponds to the ideal case. The NF4 fluence modulations induced by a single-period wavefront errors with PV value of $\lambda/4$ or $\lambda/8$ for each upstream grating are calculated, as shown in Figure 5 (a), (b, (c), and for all three gratings, as shown in Figure 5 (d). It can be seen that the modulation index is roughly proportional to the square of the PV, which is consistent with the analysis in[36]. Under the fixed optical distance to G4, for three upstream gratings, the mid-to-

https://doi.org/10.1017/hpl.2025.10050 Published online by Cambridge University Press

high spatial frequency wavefront errors lead to oscillatory distributions of modulation index, and the peak modulation index only induced by wavefront errors of characteristic periods, this is also the features of Talbot effect. On the other hand, the characteristic periods are distinct for each grating due to different propagation distance of field, for Φ_{G1}, they are 3.5mm,5-7mm with the maximum modulation index exceeds 3. For Φ_{G2}, they are 2mm, 3mm, 4.5mm, 6mm with the maximum modulation index of about 1.78. For Φ_{G3}, they are 1mm, 2mm, 2.5mm with the maximum modulation index of about 1.78. And 2.5mm,4.5-11mm with the maximum modulation index exceeds 3 for all. In addition, to limit the modulation index less than 1.5, in case of $H=\lambda/4$, the period ranges that needs to be controlled are $0.5-15\text{mm}$ for Φ_{G1}, $0.5-10\text{mm}$ for Φ_{G2}, $0.5-5\text{mm}$ for Φ_{G3} and $0.5-20\text{mm}$ for all. In the case of $H=\lambda/8$, the ranges are $0.5-12\text{mm}$ for Φ_{G1}, $0.5-15\text{mm}$ for all three gratings, for only Φ_{G2} or Φ_{G3}, all the induced modulation indices are less than 1.5. It needs to be emphasized that these ranges are obtained based on the wavefront errors of the diffracted beam, which must be divided by $\cos\beta_0$ for Φ_{G1}, Φ_{G3} or $\cos\gamma$ for Φ_{G2} to approximately transformed onto the grating plane.

In general, the maximum modulation index induced by the periodic wavefront errors of G2 and G3 is significantly lower than that of G1, G1 also possess the maximum characteristic period, confirming the influence of angular dispersion and diffraction effects described before. Besides, the result in Figure 5 (d) reveals a significant enhancement of NF4 fluence modulation at the overlapping characteristic periods of each gratings. It is worth noting that the simulation considers only single-period wavefront errors to evaluate the characteristic period ranges for NF4. However, actual fabrication typically produces wavefront with multiple periods. Calculations based on the measured wavefronts presented below suggest a better performance of the practical multiple-

https://doi.org/10.1017/hpl.2025.10050 Published online by Cambridge University Press

period wavefront errors.

3.3 NF4 fluence modulation induced by mosaic gap amplitude error

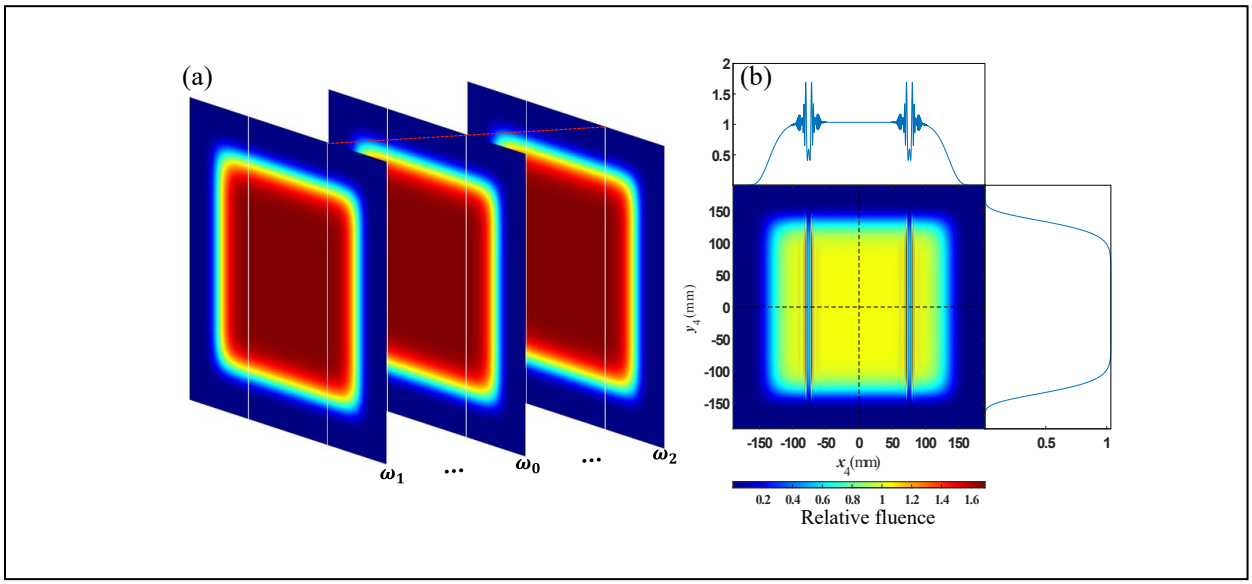

Figure 6. NF4 fluence modulation induced by gap amplitude error A_{G1}. (a) Diagram of gap amplitude error for three selected frequencies on the diffracted beam plane at G1. (b) NF4 fluence modulation induced by A_{G1}.

In the gap area of mosaic grating no exposure takes place, leading to energy loss of diffracted beam, defined as gap amplitude error. Figure 6 (a) illustrates the gap amplitude error on the diffracted beam plane at G1, as described in Section 2.3, the spatial positions of mosaic gaps are independent of ω, but the equivalent gap width varies with ω. The resulting NF4 fluence modulation is shown in Figure 6 (b), with a modulation index of 1.7, intense modulation is originated from the diffraction effects of the gap edges. The output energy is reduced to 1.178kJ, the laser peak power is decreased by approximately 1.2% from 1.127×10^{14} W to 1.113×10^{14} W, this result remains valid for the G2 and G3 gap amplitude error. Notably, the modulations induced by two gaps are independent on each other and exhibit a pattern akin to a thin opaque strip [37].

https://doi.org/10.1017/hpl.2025.10050 Published online by Cambridge University Press

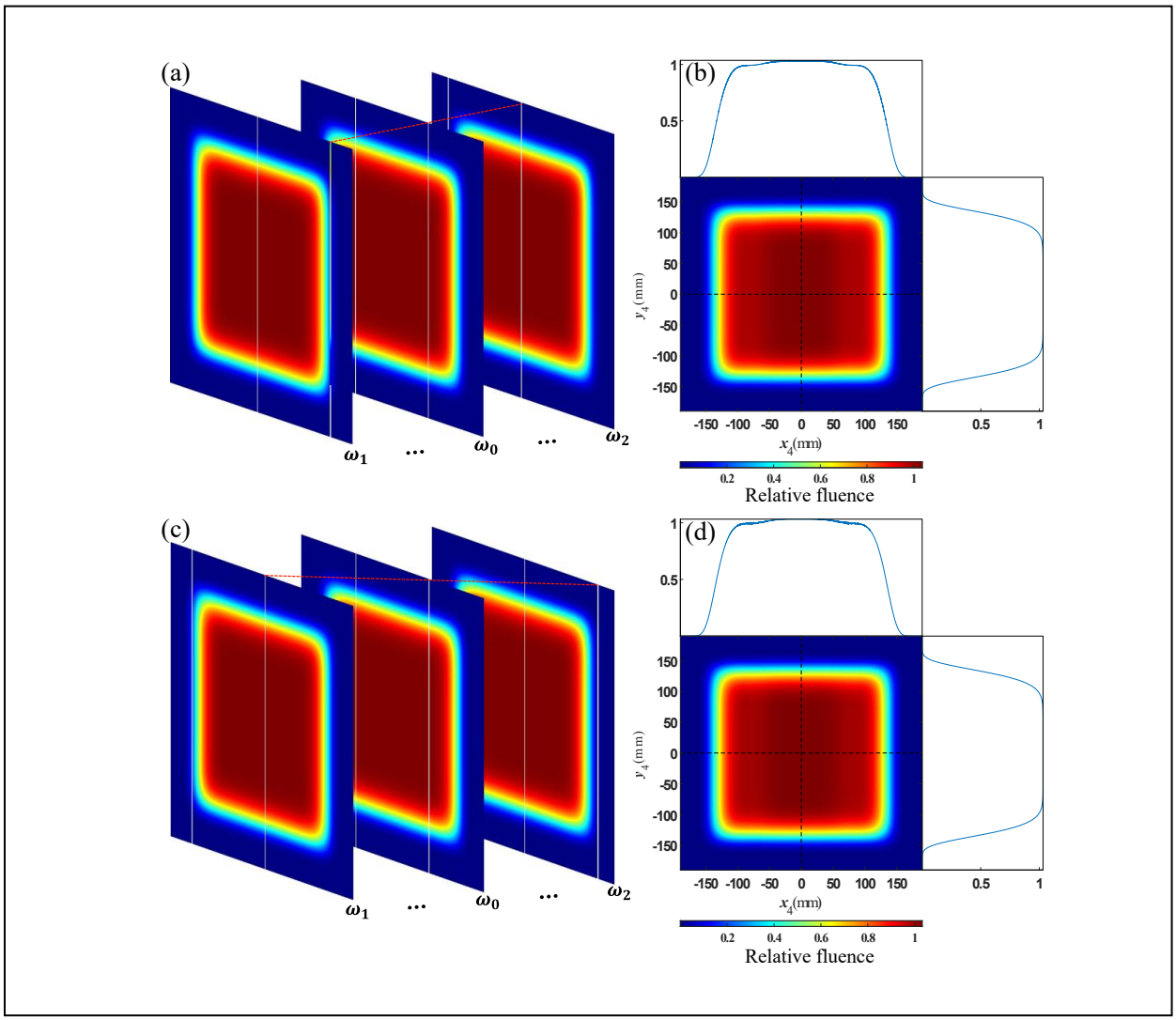

Figure 7. NF4 fluence modulation induced by gap amplitude errors A_{G2} and A_{G3}. (a) Diagram of gap amplitude error for three selected frequencies on the diffracted beam plane at G2. (b) NF4 fluence modulation induced by A_{G2}. (c) Diagram of gap amplitude error for three selected frequencies on the diffracted beam plane at G3. (d) NF4 fluence modulation induced by A_{G3}.

The amplitude error of diffracted beam caused by the gaps on grating planes at G2 and G3 are displayed in Figure 7 (a), (c), respectively. Similarly, the spatial positions of gap amplitude error for each sub-beam are dependent upon ω at G2 and G3 due to angular dispersion. As ω

https://doi.org/10.1017/hpl.2025.10050 Published online by Cambridge University Press

increase, the gap positions shift from right to left on the diffracted beam plane at G2, and shift in the opposite direction at G3, as marked by the red lines in the Figure 6. Ultimately, the NF4 fluence modulations induced by gap amplitude error of these two gratings are smoothed due to the sweep of gap positions, with two tiny depressions forming at the location of gaps, the modulation indices in two cases are almost identical, both about 1.04.

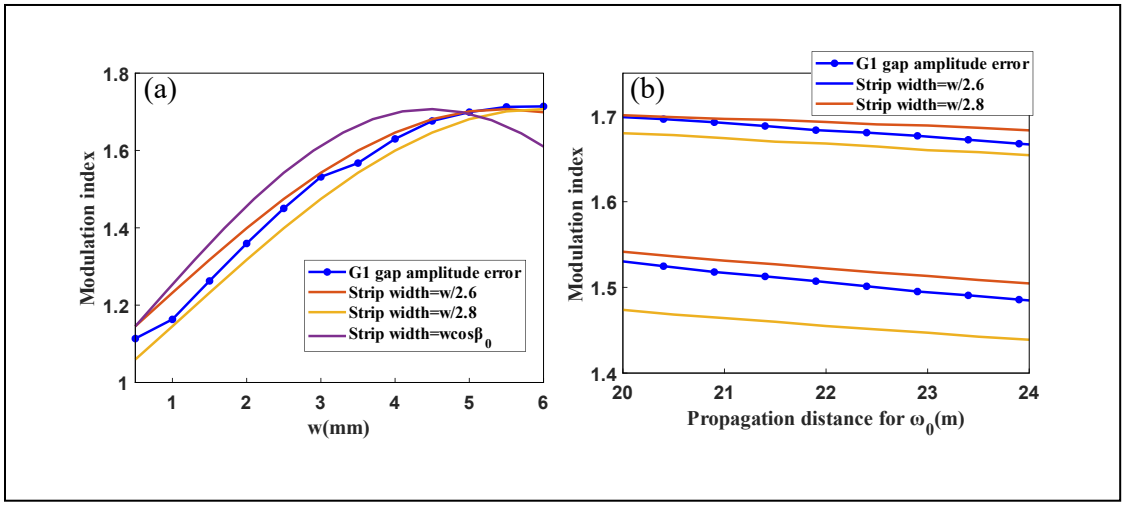

Figure 8. Comparison of the modulation index induced by diffraction of G1 mosaic gap and thin strip. (a) NF4 fluence modulation induced by A_{G1} and the modulation induced by strip diffraction for ω_0 under different w, the propagation distance is $20\mathrm{m}$. (b) The variation of the modulations with the propagation distance (up: $w=5\mathrm{mm}$, down: $w=3\mathrm{mm}$).

Figure 7 demonstrates that the gap amplitude errors of G2 and G3 possess a relatively minor impact on the NF4 comparing to that of G1. Therefore, the further analysis is only focused on G1. Considering a gap width range of $w=0.5-6\mathrm{mm}$ with an interval of $0.5\mathrm{mm}$ on the grating plane, the equivalent width on the diffracted beam plane of G1 is $w\cos\beta(\omega)$. The modulation index is calculated and shown as the blue line in Figure 8 (a). The other curves in Figure 8 (a) represent modulations induced by thin strip diffraction with three fixed strip widths of

https://doi.org/10.1017/hpl.2025.10050 Published online by Cambridge University Press

$w\cos\beta_0$, w/2.6 and w/2.8 on the beam plane under a propagation distance of 20m for ω_0, which is equal to the working-distance of Q_0=10617mm. The results reveal that the NF4 fluence modulation characteristics caused by A_{G1} closely resemble those induced by thin strip diffraction. Due to the ω-dependent equivalent width, the characteristics of NF4 fluence modulation align more closely with which of thin strip diffraction with widths of w/2.6, w/2.8, instead of a strip width of $w\cos\beta_0$ (w/2.2, approximately). Within the range of $w = 0.5-6$mm, smaller width result in lower NF4 fluence modulation, but the width of the mosaic gap is limited to $3-5$mm under the current fabrication conditions. Therefore, considering the typical cases of $w = 3$mm, 5mm, the fluence modulation induced by A_{G1} with Q_0=10617-14717mm, about 20-24m optical pathlength for ω_0, and the modulations induced by thin strip diffraction with width of w/2.6, w/2.8 under the propagation distances between 20-24m are shown in Figure 8 (b). It can be observed that changing the working-distance cannot significantly mitigate the NF4 fluence modulation induced by A_{G1}, when Q_0 is lengthened by 4m, the modulation index only decreases by about 3%.

3.4 NF4 fluence modulation induced by measured wavefront of mosaic grating

https://doi.org/10.1017/hpl.2025.10050 Published online by Cambridge University Press

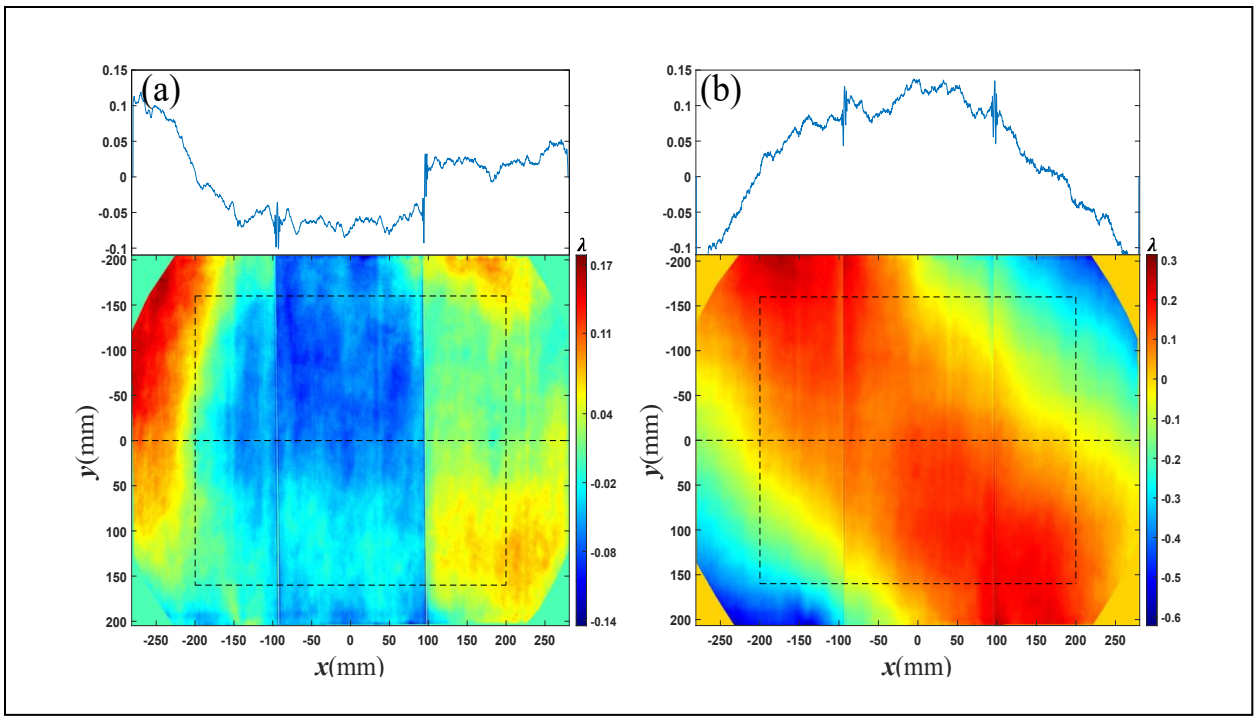

Figure 9. Two diffracted wavefronts from Littrow-mounted mosaic gratings measured by a 600mm circular-aperture interferometer. (a)The first wavefront with PV of about 0.3λ. (b) The second wavefront with PV of about 0.9λ.

To evaluate the characteristics of NF4 fluence modulation caused by phase jump across the mosaic gap, two diffracted wavefronts with phase jumps across 5mm - width gaps are introduced, which are shown in Figure 9 (a), (b). The gratings are Littrow mounted, the monochromatic probe light with λ=1053nm is diffracted to propagate along the incident path and returns to the interferometer, the four corners of measured wavefront distribution is cropped due to the interferometer possesses a circular aperture with 600mm diameter. It can be observed that the phase jump of the first wavefront is more severe, and there are mid-to-high frequency wavefront errors occur at the mosaic gaps. For the 1.4m×0.42m grating utilized in the SG-II UP PW picosecond system compressor, the Littrow angle is 66°, the length of the rectangle in lateral view

https://doi.org/10.1017/hpl.2025.10050 Published online by Cambridge University Press

is about 569mm, the resolution is 0.274mm with 1500×2050 sampling points for two wavefronts, respectively.

Based on the previous results, only considering the G1 errors with the most severe impact on the NF4 in this Section. The area enclosed by black dotted lines corresponds to the aperture of the input beam, the interpolation algorithm is adopted to increase the sampling points to 4096×4096, taking the two wavefronts as Φ_{G1}, the resulting NF4 fluence modulations are shown in Figure 10 (a), (c), respectively. It is obvious that the peak fluence modulation is induced by mid-to-high frequency wavefront error across the mosaic gap, both of the fluence modulation indices reach approximately 1.36, implying that the low frequency wavefront error almost have no effect on NF4. After introducing the amplitude error A_{G1}, the near-field modulations are displayed on Figure 10 (b, d). It can be seen that the combined effect of wavefront and amplitude errors further degrades the near-field quality, with near-field modulation index has reached 1.9 for the first wavefront and 1.8 for the second. Notably, the first wavefront, which has a smaller PV value, results in a higher modulation index than the second wavefront, this phenomenon is caused by the worse continuity across the gap of the first wavefront. Furthermore, referring to Figure 6, Figure 7, Figuer 8 and Figure 10, it is evident that the near-field modulation induced by G1 gap amplitude error is dominant under the current status, confirming that controlling the mosaic gap width of G1 is an effective approach to mitigate near-field modulation.

https://doi.org/10.1017/hpl.2025.10050 Published online by Cambridge University Press

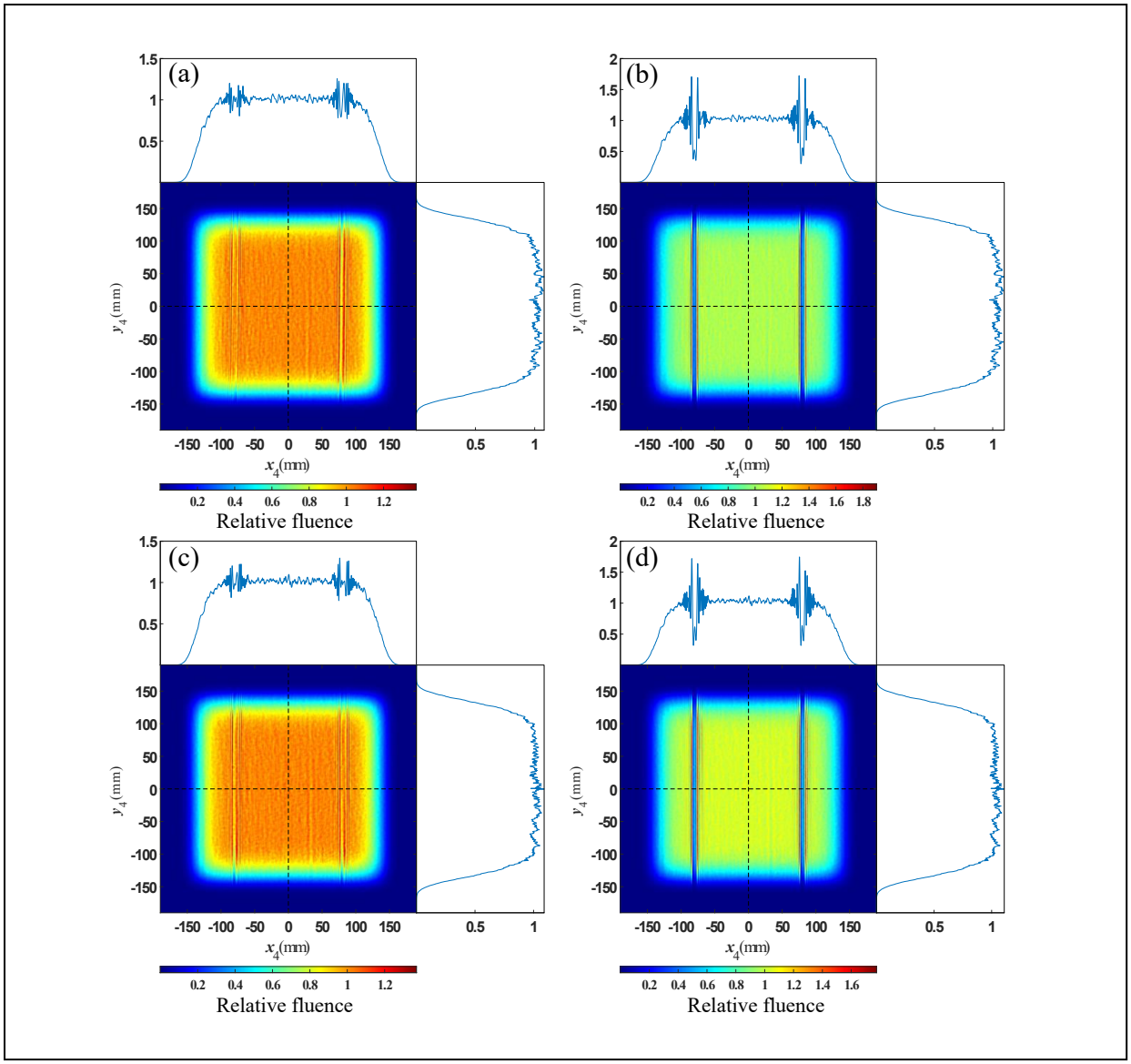

Figure 10. NF4 fluence modulation induced by (a)The first wavefront without A_{G1}, (b) Both the first wavefront and A_{G1}, (c) The second wavefront without A_{G1}, (d) Both the second wavefront and A_{G1}.

IV. CONCLUSION

To better understand the near-field propagation properties within the mosaic grating based compressor, based on ray tracing and diffraction propagation theory, we proposed a 3D near-field

https://doi.org/10.1017/hpl.2025.10050 Published online by Cambridge University Press

propagation model for the SG-II UP PW picosecond system compressor. Focusing on the periodic wavefront error and mosaic gap error under the laser pulse with narrowband, we investigate the characteristics of NF4 fluence modulation induced by the errors of the first three gratings respectively. The results indicate that the errors of G1 have the most significant impact on NF4. In severe cases, the mid-to-high frequency single-period wavefront errors of $T = 0.5 - 15\text{mm}$ at G1 can increase NF4 fluence modulation index to 3, but just about 1.8 for G2 and G3 due to the smoothing along the dispersion direction of NF4 fluence modulation caused by angular dispersion. These smoothing effects also significantly mitigate the NF4 fluence modulations induced by gap amplitude error of G2 and G3. Besides, the periods of G1 diffracted wavefront along the x direction must be divided by $\cos\beta_0$ to approximately transformed onto the grating plane. For gap amplitude error of G1, the simulation highlights the control of mosaic gap width, under current fabrication conditions, a gap width of 3mm is recommended. Relying on two diffracted wavefronts measured by an interferometer, we preliminarily identify that the phase discontinuity across G1 gap can magnify the NF4 fluence modulation induced by gap amplitude error, to mitigate this effect, a continuous wavefront is recommended. In summary, it is recommended to use a grating with the highest quality diffracted wavefront as G1. Notably, the errors of G1 can be equivalent to the input pulse errors, underscoring the importance of precise control for the phase and amplitude of the input pulse. The simulation model can also be used to optimize the positions of other downstream optics, such as following transport mirrors. Moreover, this study does not address the composite impact of gap amplitude errors of all gratings, which is more reflective of the reality, further investigation is warranted.

Acknowledgement

https://doi.org/10.1017/hpl.2025.10050 Published online by Cambridge University Press

The authors would like to thank the staffs of the NLHPLP and the joint researching team of meter-scale grating. This work was supported by Strategic Priority Research Program of the Chinese Academy of Sciences (XDA25020203).

References

1. M. Bailly-Grandvaux, D. Kawahito, C. McGuffey, J. Strehlow, B. Edghill, M. S. Wei, N. Alexander, A. Haid, C. Brabetz, V. Bagnoud, R. Hollinger, M. G. Capeluto, J. J. Rocca, and F. N. Beg, "Ion acceleration from microstructured targets irradiated by high-intensity picosecond laser pulses," Physical Review E 102, 021201 (2020). DOI: https://doi.org/10.1103/PhysRevE.102.021201
2. F. Zhang, H. B. Cai, W. M. Zhou, Z. S. Dai, L. Q. Shan, H. Xu, J. B. Chen, F. J. Ge, Q. Tang, W. S. Zhang, L. Wei, D. X. Liu, J. F. Gu, H. B. Du, B. Bi, S. Z. Wu, J. Li, F. Lu, H. Zhang, B. Zhang, M. Q. He, M. H. Yu, Z. H. Yang, W. W. Wang, H. S. Zhang, B. Cui, L. Yang, J. F. Wu, W. Qi, L. H. Cao, Z. Li, H. J. Liu, Y. M. Yang, G. L. Ren, C. Tian, Z. Q. Yuan, W. D. Zheng, L. F. Cao, C. T. Zhou, S. Y. Zou, Y. Q. Gu, K. Du, Y. K. Ding, B. H. Zhang, S. P. Zhu, W. Y. Zhang, and X. T. He, "Enhanced energy coupling for indirect-drive fast-ignition fusion targets," Nature Physics 16, 810-814 (2020). DOI: https://doi.org/10.1038/s41567-020-0878-9
3. H. Hora, G. H. Miley, X. Yang, and P. Lalousis, "Strong shock-phenomena at petawatt-picosecond laser side-on ignition fusion of uncompressed hydrogen-boron11," Astrophysics and Space Science 336, 225-228 (2011). DOI: https://doi.org/10.1007/s10509-011-0681-2
4. K. Lezhnin, "Using High Power Lasers as a Tool for Secondary Sources and Laboratory Astrophysics," Ph.D. (Princeton University, United States -- New Jersey, 2022). https://www.proquest.com/dissertations-theses/using-high-power-lasers-as-tool-secondary-sources/docview/2742664832/se-2?accountid=178558
5. D. Strickland and G. Mourou, "Compression of amplified chirped optical pulses," Optics Communications 55, 447-449 (1985). DOI: https://doi.org/https://doi.org/10.1016/0030-4018(85)90151-8
6. T. J. Kessler, J. Bunkenburg, H. Huang, A. Kozlov, and D. D. Meyerhofer, "Demonstration of coherent addition of multiple gratings for high-energy chirped-pulse-amplified lasers," Opt. Lett. 29, 635-637 (2004). DOI: https://doi.org/10.1364/OL.29.000635
7. L. Shi, L. Zeng, and L. Li, "Fabrication of optical mosaic gratings with phase and attitude adjustments employing latent fringes and a red-wavelength dual-beam interferometer," Opt. Express 17, 21530-21543 (2009). DOI: https://doi.org/10.1364/OE.17.021530
8. M. S. Hur, B. Ersfeld, H. Lee, H. Kim, K. Roh, Y. Lee, H. S. Song, M. Kumar, S. Yoffe, D. A. Jaroszynski, and H. Suk, "Laser pulse compression by a density gradient plasma for exawatt to zettawatt lasers," Nature Photonics 17, 1074-1079 (2023). DOI: https://doi.org/10.1038/s41566-023-01321-x
9. K. D. Chesnut and C. P. J. Barty, "Ideal spatio-temporal pulse distribution for exawatt-scale lasers based on simultaneous chirped beam and chirped pulse amplification," Opt. Express 31, 5687-5698 (2023). DOI: https://doi.org/10.1364/OE.480302

https://doi.org/10.1017/hpl.2025.10050 Published online by Cambridge University Press

10. W. H. Williams, J. K. Crane, D. A. Alessi, C. D. Boley, M. W. Bowers, A. D. Conder, J.-M. G. Di Nicola, P. Di Nicola, C. Haefner, J. M. Halpin, M. Y. Hamamoto, J. E. Heebner, M. R. Hermann, S. I. Herriot, D. C. Homoelle, D. H. Kalantar, T. E. Lanier, K. N. LaFortune, J. K. Lawson, R. R. Lowe-Webb, F. X. Morrissey, H. Nguyen, C. D. Orth, L. J. Pelz, M. A. Prantil, M. C. Rushford, R. A. Sacks, J. T. Salmon, L. G. Seppala, M. J. Shaw, R. J. Sigurdsson, P. J. Wegner, C. C. Widmayer, S. T. Yang, and T. L. Zobrist, "Spatio-temporal focal spot characterization and modeling of the NIF ARC kilojoule picosecond laser," Appl. Opt. 60, 2288-2303 (2021). DOI: https://doi.org/10.1364/AO.416846
11. N. Blanchot, G. Marre, J. Néauport, E. Sibé, C. Rouyer, S. Montant, A. Cotel, C. Le Blanc, and C. Sauteret, "Synthetic aperture compression scheme for a multipetawatt high-energy laser," Appl. Opt. 45, 6013-6021 (2006). DOI: https://doi.org/10.1364/AO.45.006013
12. J. Qiao, A. Kalb, T. Nguyen, J. Bunkenburg, D. Canning, and J. H. Kelly, "Demonstration of large-aperture tiled-grating compressors for high-energy, petawatt-class, chirped-pulse amplification systems," Opt. Lett. 33, 1684-1686 (2008). DOI: https://doi.org/10.1364/OL.33.001684
13. D. Smith, M. McCullough, C. Smith, T. Mikami, and T. Jitsuno, *Low stress ion-assisted coatings on fused silica substrates for large aperture laser pulse compression gratings*, Boulder Damage Symposium XL Annual Symposium on Optical Materials for High Power Lasers (SPIE, 2008), Vol. 7132.
14. J. Zhu, J. Zhu, X. Li, B. Zhu, W. Ma, X. Lu, W. Fan, Z. Liu, S. Zhou, G. Xu, G. Zhang, X. Xie, L. Yang, J. Wang, X. Ouyang, L. Wang, D. Li, P. Yang, Q. Fan, M. Sun, C. Liu, D. Liu, Y. Zhang, H. Tao, M. Sun, P. Zhu, B. Wang, Z. Jiao, L. Ren, D. Liu, X. Jiao, H. Huang, and Z. Lin, "Status and development of high-power laser facilities at the NLHPLP," High Power Laser Science and Engineering 6, e55 (2018). DOI: https://doi.org/10.1017/hpl.2018.46
15. G. Xu, T. Wang, Z. Li, Y. Dai, Z. Lin, Y. Gu, and J. Zhu, "1 kJ Petawatt Laser System for SG-II-U Program," レーザー研究 36, 1172-1175 (2008). DOI: https://doi.org/10.2184/lsj.36.1172
16. G. Qian, J. Wu, and C. Li, "Parallel Splicing Method for Holographic Gratings," Acta Optica Sinica 42(2022). DOI: https://doi.org/10.3788/AOS202242.2105002
17. Z. Li, K. Tsubakimoto, H. Yoshida, Y. Nakata, and N. Miyanaga, "Degradation of femtosecond petawatt laser beams: Spatio-temporal/spectral coupling induced by wavefront errors of compression gratings," Applied Physics Express 10, 102702 (2017). DOI: https://doi.org/10.7567/APEX.10.102702
18. Š. Vyhlídka, "Dispersion management of a 10 PW laser system," (2020). DOI:
19. J. Qiao, A. Kalb, M. J. Guardalben, G. King, D. Canning, and J. H. Kelly, "Large-aperture grating tiling by interferometry for petawatt chirped-pulse-amplification systems," Opt. Express 15, 9562-9574 (2007). DOI: https://doi.org/10.1364/OE.15.009562
20. S. Zhang, J. W. Zhang, Y. Zhou, J. Q. Su, X. Wang, B. Deng, and D. X. Hu, "Analysis of wavefront effects for large-aperture tiled-grating compressor," Laser and Particle Beams 36, 84-91 (2018). DOI: https://doi.org/10.1017/S0263034617000878
21. A. Le Camus, H. Coic, N. Blanchot, S. Bouillet, E. Lavastre, M. Mangeant, C. Rouyer, and J. Néauport, "Impact of compression grating phase modulations on beam over-intensities and downstream optics on PETAL facility," Opt. Express 30, 7426-7440 (2022). DOI: https://doi.org/10.1364/OE.449397

https://doi.org/10.1017/hpl.2025.10050 Published online by Cambridge University Press

22. B. Ashe, C. Giacofei, G. Myhre, and A. Schmid, *Optimizing a cleaning process for multilayer dielectric (MLD) diffraction gratings*, Boulder Damage Symposium XXXIX: Annual Symposium on Optical Materials for High Power Lasers (SPIE, 2007), Vol. 6720.
23. F. Koch, D. Lehr, and T. Glaser, *Stability requirements for two-beam interference lithography diffraction grating manufacturing*, SPIE Optifab (SPIE, 2017), Vol. 10448.
24. T. Zhang, M. Yonemura, and Y. Kato, "An array-grating compressor for high-power chirped-pulse amplification lasers," Optics Communications 145, 367-376 (1998). DOI: https://doi.org/https://doi.org/10.1016/S0030-4018(97)00356-8
25. H. Huang and T. Kessler, "Tiled-grating compressor with uncompensated dispersion for near-field-intensity smoothing," Opt. Lett. 32, 1854-1856 (2007). DOI: https://doi.org/10.1364/OL.32.001854
26. E. Treacy, "Optical pulse compression with diffraction gratings," IEEE Journal of Quantum Electronics 5, 454-458 (1969). DOI: https://doi.org/10.1109/JQE.1969.1076303
27. D. Homoelle, J. K. Crane, M. Shverdin, C. L. Haefner, and C. W. Siders, "Phasing beams with different dispersions and application to the petawatt-class beamline at the National Ignition Facility," Appl. Opt. 50, 554-561 (2011). DOI: https://doi.org/10.1364/AO.50.000554
28. N. Bonod and J. Neauport, "Diffraction gratings: from principles to applications in high-intensity lasers," Adv. Opt. Photon. 8, 156-199 (2016). DOI: https://doi.org/10.1364/AOP.8.000156
29. O. E. Martinez, "Grating and prism compressors in the case of finite beam size," J. Opt. Soc. Am. B 3, 929-934 (1986). DOI: https://doi.org/10.1364/JOSAB.3.000929
30. J. W. Goodman, *Introduction to Fourier optics*, (Roberts and Company publishers, Englewood, 2005).
31. E. Khazanov, "Wavefront distortions of a laser beam reflected from a diffraction grating with imperfect surface and groove pattern," Opt. Express 32, 46310-46321 (2024). DOI: https://doi.org/10.1364/OE.542565
32. Z. Li and N. Miyanaga, "Simulating ultra-intense femtosecond lasers in the 3-dimensional space-time domain," Opt. Express 26, 8453-8469 (2018). DOI: https://doi.org/10.1364/OE.26.008453
33. M. Trentelman, I. N. Ross, and C. N. Danson, "Finite size compression gratings in a large aperture chirped pulse amplification laser system," Appl. Opt. 36, 8567-8573 (1997). DOI: https://doi.org/10.1364/AO.36.008567
34. K. Mikhail, A. Alexander, and S. Horst, "Limits of the temporal contrast for CPA lasers with beams of high aperture," in *Proc.SPIE*, 2009), 750104.
35. S. Li, P. Du, F. Wu, L. Ding, Z. Lu, Y. Wang, C. An, and X. Cui, "Study of evaluating nearfield beam quality of the high power laser beams," Optik 157, 148-155 (2018). DOI: https://doi.org/https://doi.org/10.1016/j.ijleo.2017.11.079
36. P. Zhou and J. H. Burge, "Analysis of wavefront propagation using the Talbot effect," Appl. Opt. 49, 5351-5359 (2010). DOI: https://doi.org/10.1364/AO.49.005351
37. M. Wichtowski, "Simple analytic expressions of Fresnel diffraction patterns at a straight strip and slit for Gaussian wave illumination," American Journal of Physics 87, 171-175 (2019). DOI: https://doi.org/10.1119/1.5089415

https://doi.org/10.1017/hpl.2025.10050 Published online by Cambridge University Press

Figures and tables

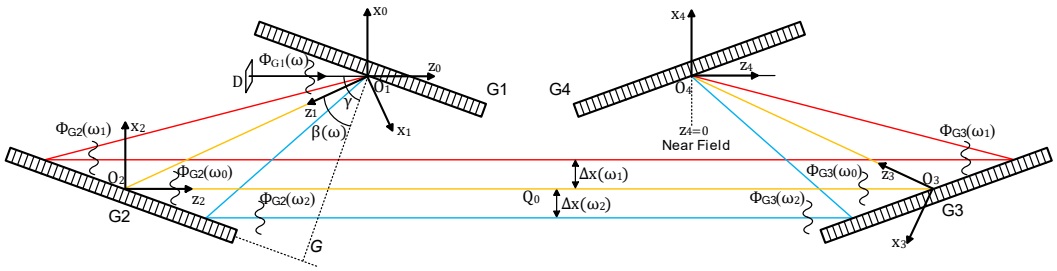

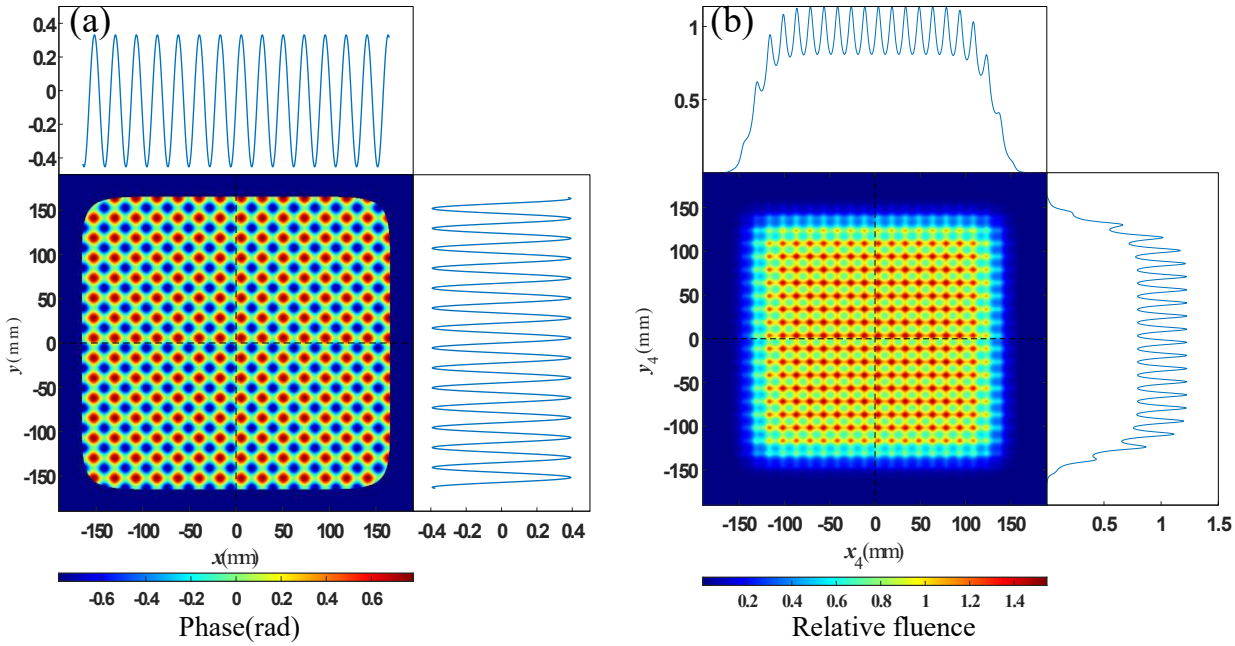

https://doi.org/10.1017/hpl.2025.10050 Published online by Cambridge University Press

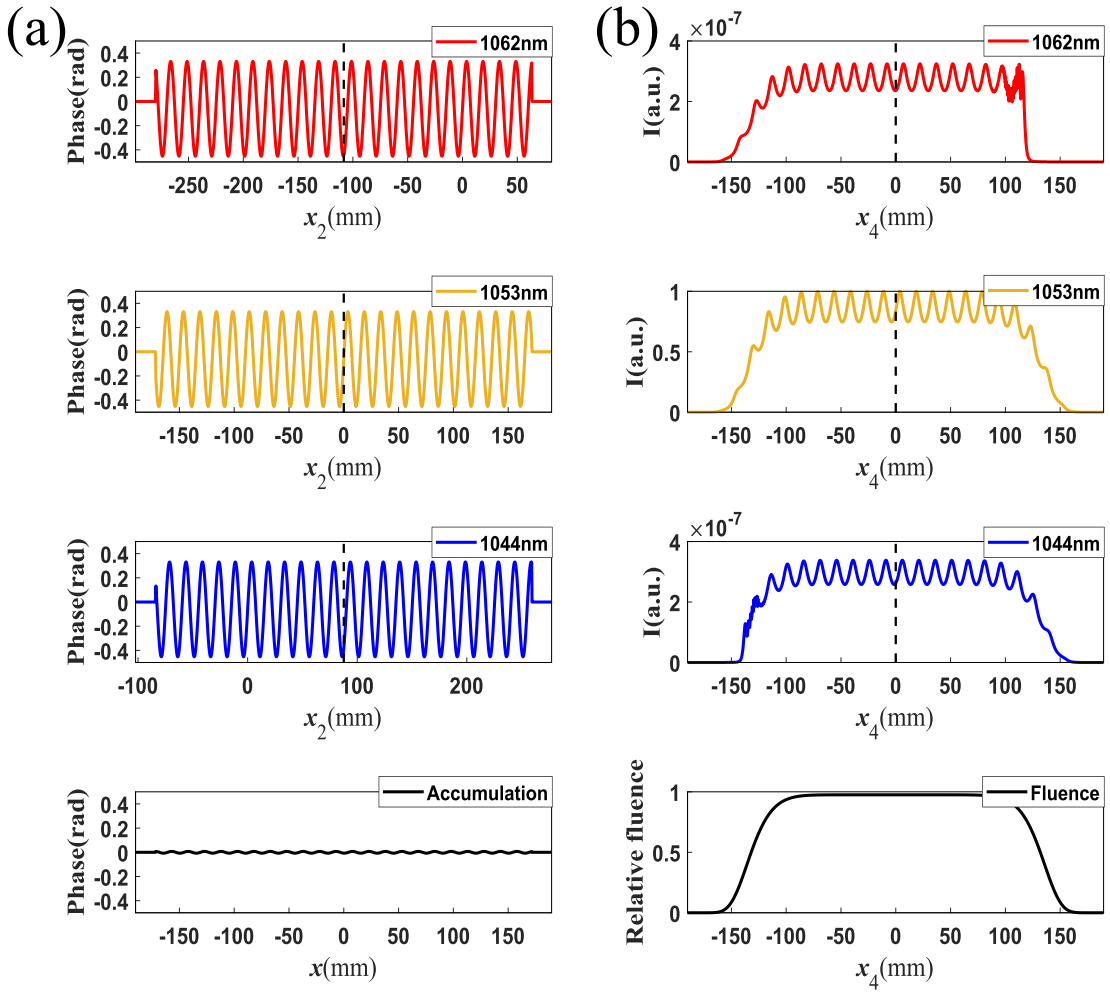

1

https://doi.org/10.1017/hpl.2025.10050 Published online by Cambridge University Press

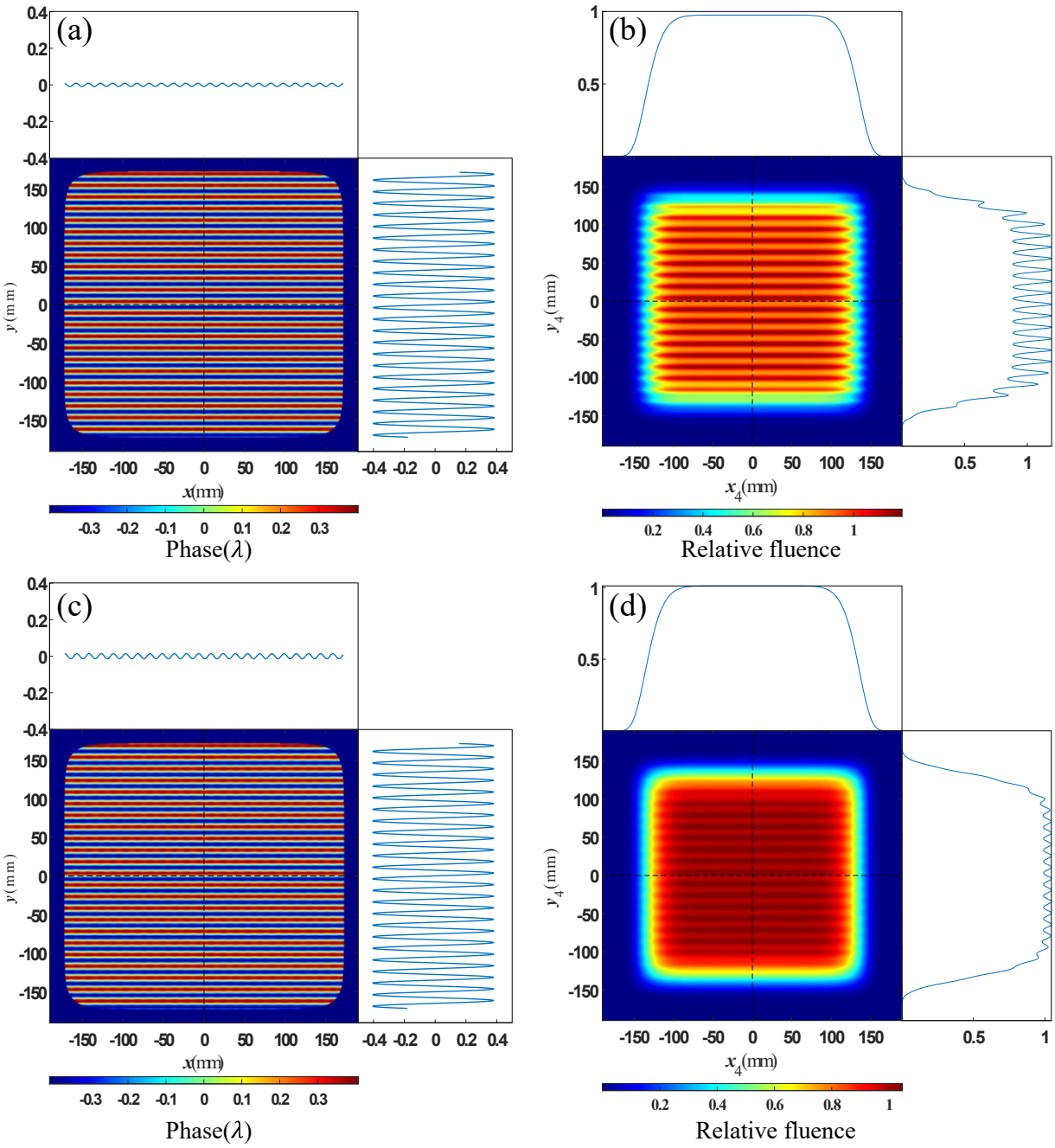

1

2

https://doi.org/10.1017/hpl.2025.10050 Published online by Cambridge University Press

1

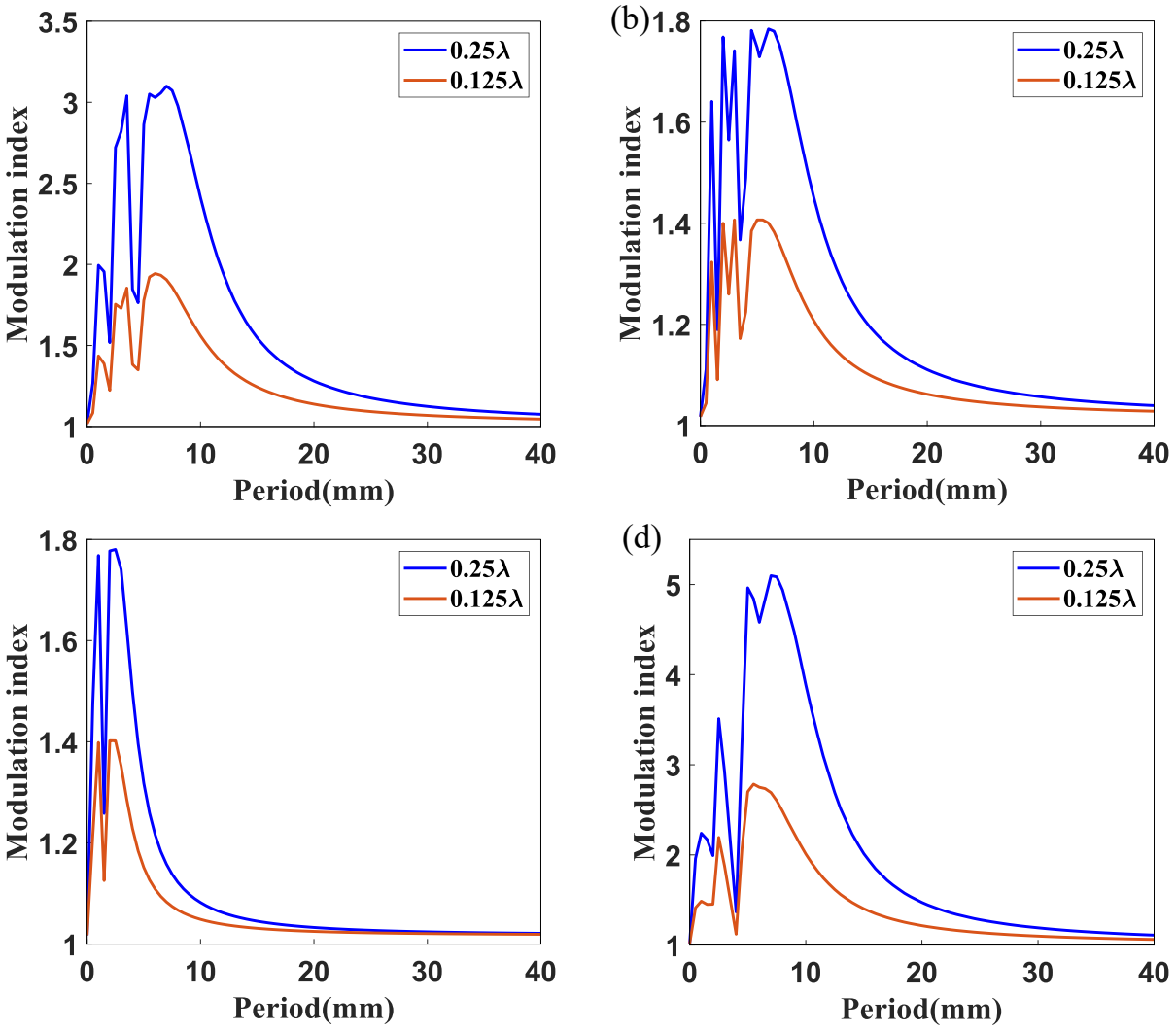

2

3

https://doi.org/10.1017/hpl.2025.10050 Published online by Cambridge University Press

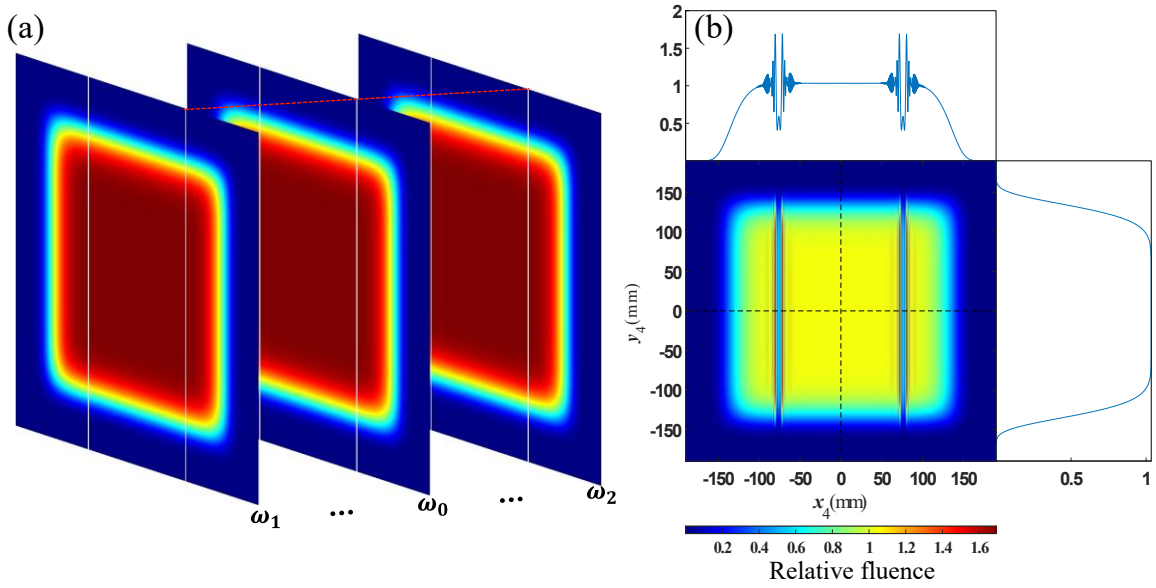

1

https://doi.org/10.1017/hpl.2025.10050 Published online by Cambridge University Press

1

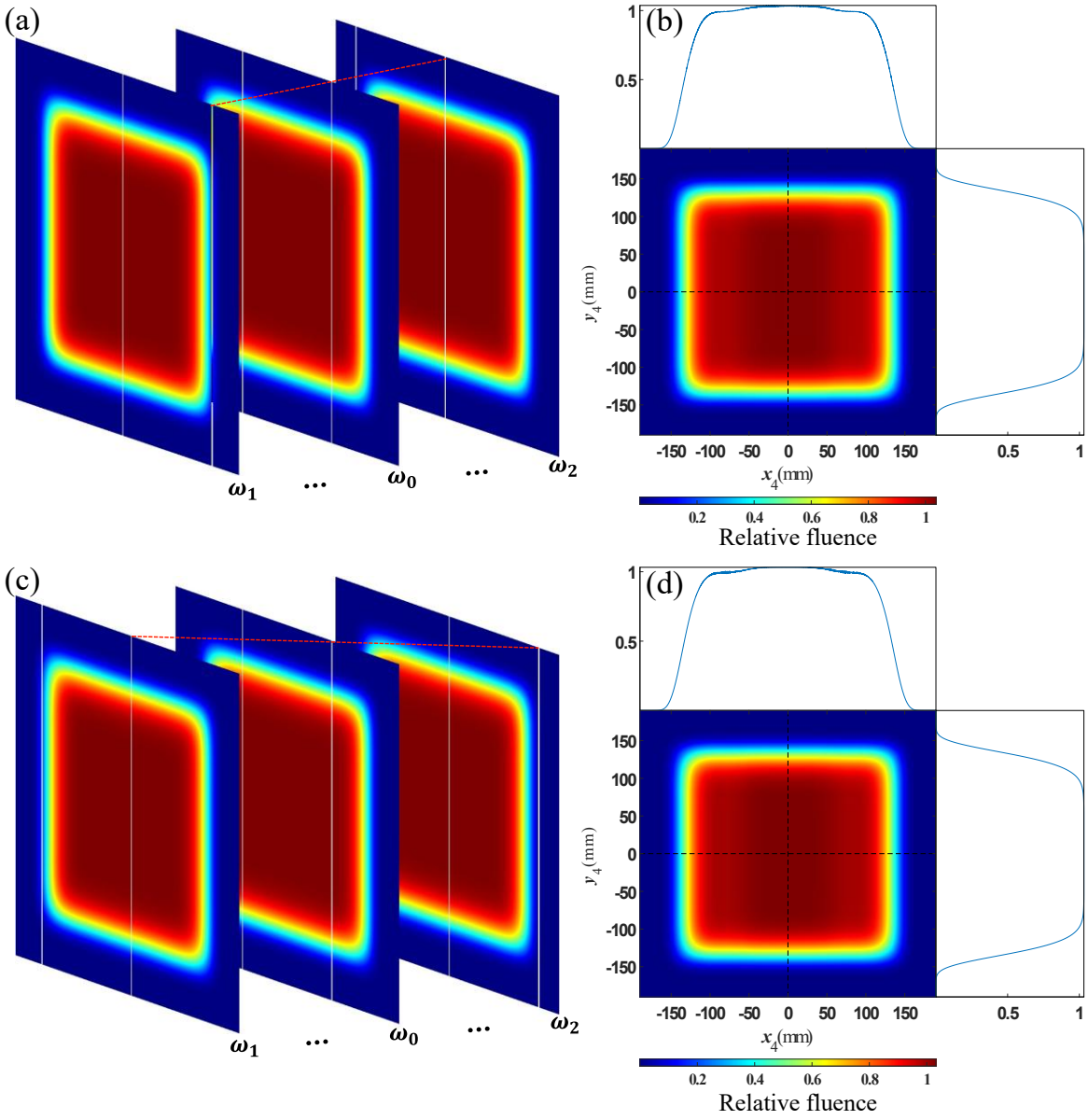

2

https://doi.org/10.1017/hpl.2025.10050 Published online by Cambridge University Press

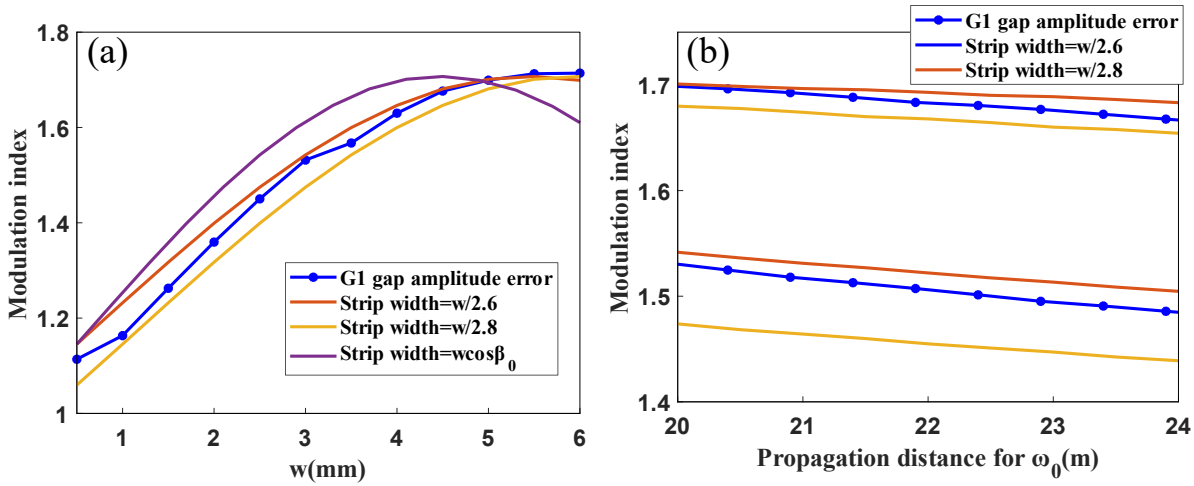

1

2

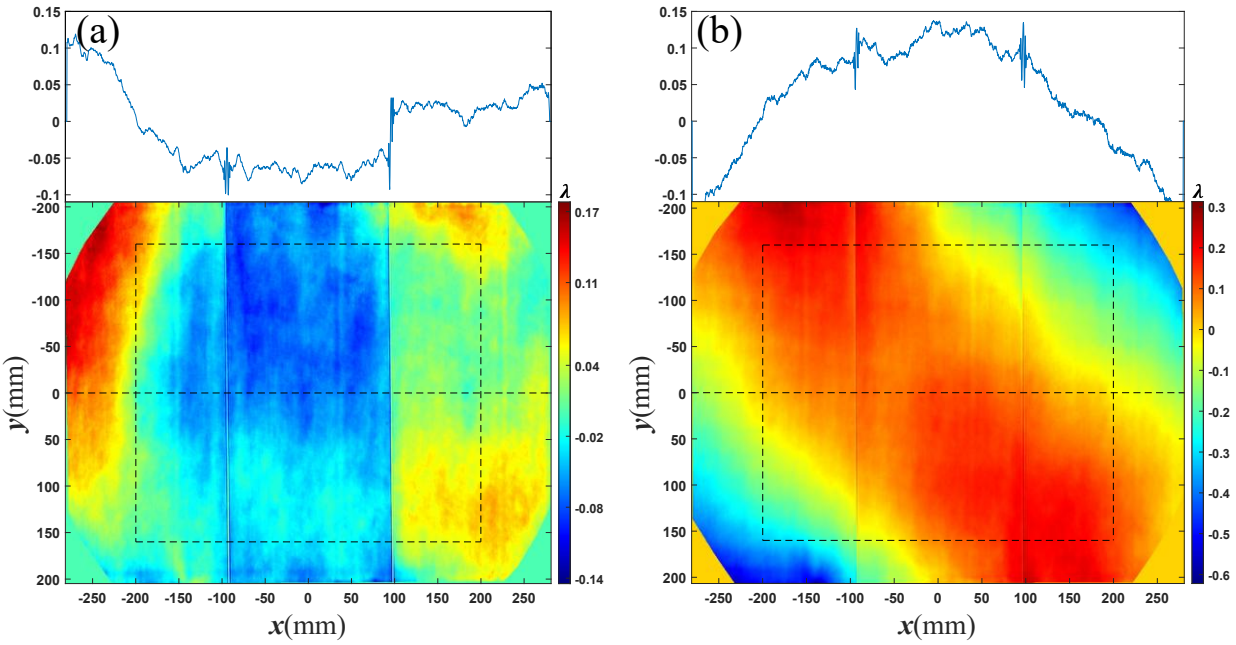

3

4

https://doi.org/10.1017/hpl.2025.10050 Published online by Cambridge University Press

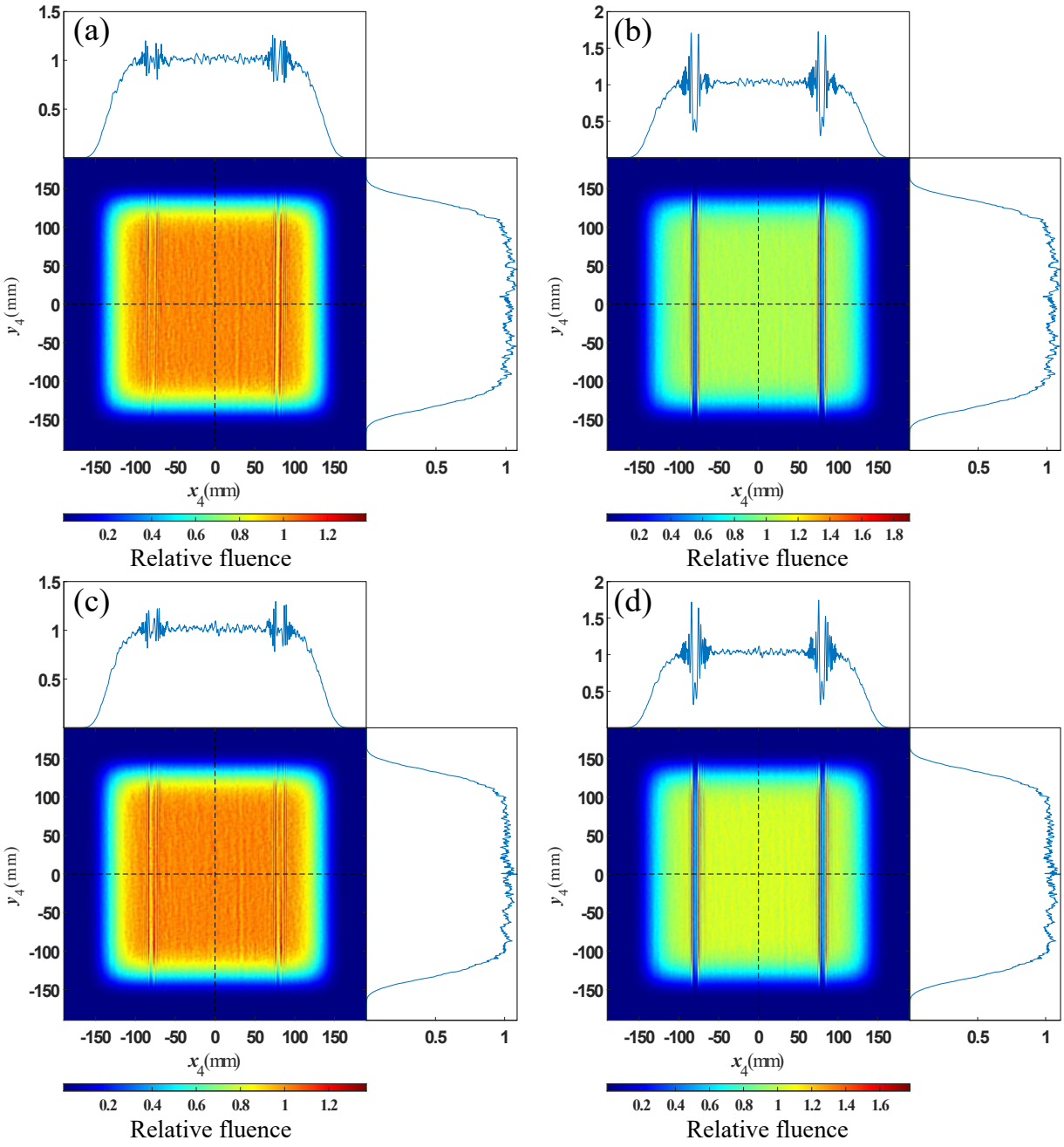

Figure and table captions

Figure 1. Schematic of broadband pulse propagation model for grating compressor.

Figure 2. NF4 fluence modulation induced by the periodic wavefront error Φ_{G1} with T=15mm, H=λ/4. (a) Accumulation of Φ_{G1} over ω. (b) NF4 fluence modulation induced by Φ_{G1}.

https://doi.org/10.1017/hpl.2025.10050 Published online by Cambridge University Press

Figure 3. NF4 fluence modulation induced by the periodic wavefront errors Φ_{G2} or Φ_{G3} with $T = 15\text{mm}, H = \lambda/4$. (a) Accumulation of Φ_{G2} over ω in the same aperture. (b) NF4 fluence modulation induced by Φ_{G2}. (c) Accumulation of Φ_{G3} over ω in the same aperture. (d) NF4 fluence modulation induced by Φ_{G3}.

Figure 4. (a) The distributions of Φ_{G2} along the x_2 direction with $y_2 = 0$ for different wavelengths, the black line represents the accumulated result of Φ_{G2}. (b) The resulting NF4 intensity distribution in different wavelengths along the x_4 direction with $y_4 = 0$, and the fluence along x_4 direction is displayed at the bottom.

Figure 5. NF4 fluence modulation induced by (a) Φ_{G1}, (b) Φ_{G2}, (c) Φ_{G3}, (d) periodic wavefront errors of all upstream gratings, with $T = 0.5 - 40\text{mm}, H = \lambda/4$ or $\lambda/8$.

Figure 6. NF4 fluence modulation induced by gap amplitude error A_{G1}. (a) Diagram of gap amplitude error for three selected frequencies on the diffracted beam plane at G1. (b) NF4 fluence modulation induced by A_{G1}.

Figure 7. NF4 fluence modulation induced by gap amplitude errors A_{G2} and A_{G3}. (a) Diagram of gap amplitude error for three selected frequencies on the diffracted beam plane at G2. (b) NF4 fluence modulation induced by A_{G2}. (c) Diagram of gap amplitude error for three selected frequencies on the diffracted beam plane at G3. (d) NF4 fluence modulation induced by A_{G3}.

Figure 8. Comparison of the modulation index induced by diffraction of G1 mosaic gap and thin strip. (a) NF4 fluence modulation induced by A_{G1} and the modulation induced by strip diffraction for ω_0 under different w, the propagation distance is 20m. (b) The variation of the modulations with the propagation distance (up: $\mathrm{w}=5\text{mm}$, down: $\mathrm{w}=3\text{mm}$).

Figure 9. Two diffracted wavefronts from Littrow-mounted gratings measured by a 600mm circular-aperture interferometer. (a)The first wavefront with PV of about 0.3λ. (b) The second

https://doi.org/10.1017/hpl.2025.10050 Published online by Cambridge University Press

wavefront with PV of about 0.9λ.

Figure 10. NF4 fluence modulation induced by (a)The first wavefront only, (b) Both the first wavefront and gap amplitude error, (c) The second wavefront only, (d) Both the second wavefront and gap amplitude error of G1.

https://doi.org/10.1017/hpl.2025.10050 Published online by Cambridge University Press